The Journal of Physical Chemistry Letters

Letter

Cite This: J. Phys. Chem. Lett. 2019, 10, 7774−7780

pubs.acs.org/JPCL

Self-Healing of Photocurrent Degradation in Perovskite Solar Cells: The Role of Defect-Trapped Excitons

Guangjun Nan,[†] Xu Zhang,[‡] and Gang Lu*,[‡]

[†]Department of Physics, Zhejiang Normal University, Jinhua 321004, China

[‡]Department of Physics and Astronomy, California State University, Northridge, Northridge, California 91330-8268, United States

Supporting Information

ABSTRACT: Solution-processed lead halide perovskites have emerged as one of the most promising materials in optoelectronic applications. However, the perovskites are not stable over prolonged solar illumination. A recent experimental study has revealed light-activated photocurrent degradation and self-healing in lead halide perovskites, which has important implications in tackling the photostability problems of the perovskites. Unfortunately, the physical origin of the experimental observations is unclear. In this work, we propose a first-principles theory that can elucidate all key experimental observations. By focusing on defect-trapped excitons, the theory can rationalize both fast and slow time scales of self-healing, contrasting dynamics of the photocurrent degradation and its recovery, and the steep temperature dependence of the two competing processes. We further predict that the same phenomenon of self-healing could also be observed in other lead halide perovskites with even faster time scales of recovery. The work provides a general framework for elucidating defect-controlled excitation dynamics in perovskites.

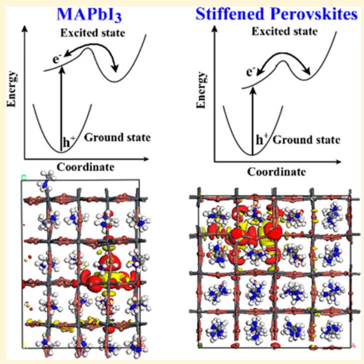

Lead halide perovskites (LHPs) have recently emerged as a class of highly promising materials for optoelectronic applications, ranging from photovoltaics[1,2] to light-emitting diodes[3,4] and optically pumped lasers.[5] Crystallized in corner-sharing octahedra with cages, three-dimensional LHPs bear a general chemical formula of ABX_3, with a large organic cation ("A") occupying the center of each cage, a lead cation ("B") at the center of each octahedron, and halide anions ("X") taking the corners of the octahedron.[6] Within only a few years, LHPs have achieved a power conversion efficiency (PCE) of 25.2%,[7] which is a truly remarkable feat given the fact that these perovskites are often solution-processed. Despite the achievements, however, LHPs suffer from critical stability problems; they are sensitive to water moisture,[8,9] ultraviolet light,[10,11] and thermal stress,[12] which represents a major roadblock to their commercialization. While exposure to moisture may be alleviated through encapsulation of the devices,[13,14] the problem of photostability remains highly challenging and far from being resolved.[15−17]

Nonetheless, much progress has been made to address the photostability problems.[18,19] For example, earlier work has focused on the role of light-triggered ion migration in the photostability of the perovskites.[20−22] Among the recent efforts, the discovery of light-activated photocurrent degradation and self-healing in $MAPbI_3$ (MA = CH_3NH_3) is particularly interesting with far-reaching implications.[23] The researchers demonstrated that the degradation of the photovoltaic performance under constant solar illumination was due to the reduction of the photocurrent, which, crucially, can rapidly recover or self-heal in the dark to its original value. Two distinct recovery time regimes were observed: a fast recovery (<1 min), which brings the device to ~96% of its steady-state value, followed by a longer recovery time (tens of minutes to an hour) to fully restore the device photocurrent. The photocurrent degradation was attributed to the formation of deep trap states (>0.5 eV), which are light-activated and metastable. While both the degradation and self-healing of the devices were highly sensitive to temperature, the dynamics of the former (in hours) is much slower than the latter (in minutes). Finally, a decrease in the open circuit voltage (V_{oc}) by 40 mV was observed and attributed to the existence of the deep trap states. The authors proposed that the formation of small polarons is responsible for the experimental observations based on the following considerations. (1) Localized polaronic states can manifest as deep trap states within the band gap, which over time lead to the accumulation of space charges and a ≤40% decrease in the photocurrent. (2) The formation of small polarons is not expected to be extremely fast, but faster than the observed time scales in the degradation of the devices. (3) The slow degradation of the photocurrent is attributed to the very slow mobility and the accumulation of the small polarons. Although these considerations are fairly reasonable, the proposal cannot explain the two most crucial aspects of the experiments: (1) self-healing and the time scales for self-healing. The first-principles calculations by these authors revealed that the binding energy of small polarons in $MAPbI_3$ is on the order of 600 meV (hole polaron) and 1300 meV (electron polaron), which is much higher than the thermal

Received: November 19, 2019
Accepted: December 2, 2019
Published: December 2, 2019

DOI: 10.1021/acs.jpclett.9b03413
J. Phys. Chem. Lett. 2019, 10, 7774−7780

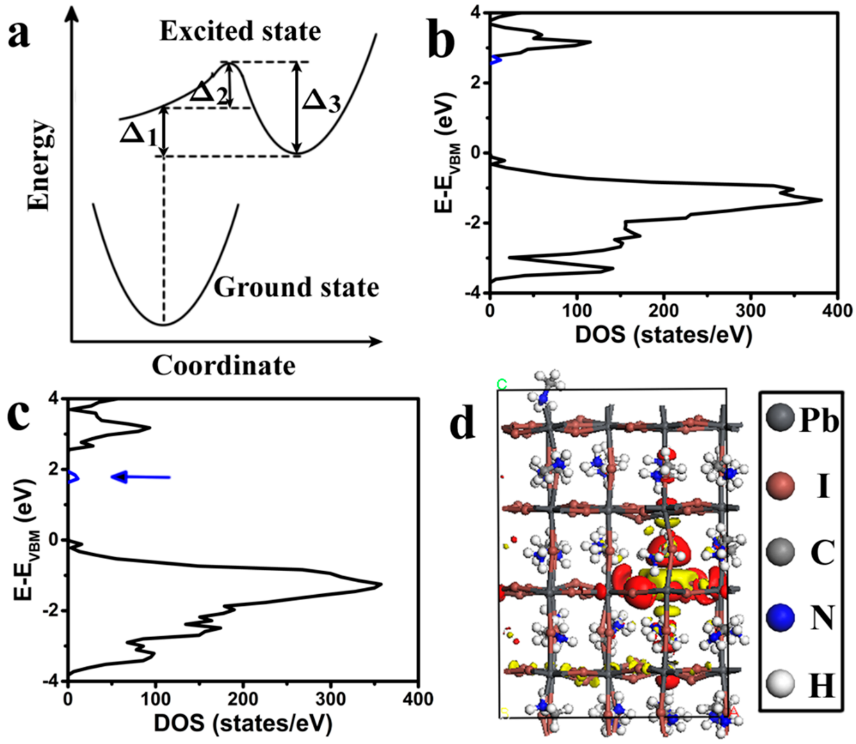

Figure 1. (a) Sketch of the potential energy surfaces in the electronic ground state and the lowest excited state for $MAPbI_3$ in the presence of iodine vacancies. Δ_1 represents the excitation energy difference between the equilibrium geometries in the ground state and the excited state. Δ_2 represents the trapping energy barrier, and Δ_3 represents the detrapping energy barrier. (b) DOS of the system before the forward relaxation with shallow defect levels colored blue. The valence band maximum is denoted as VBM. (c) DOS after the forward relaxation with the deep trap states colored blue. The DOS in panels b and c are calculated with the OT-RSH functional. (d) Exciton charge density with the electron (hole) density colored red (yellow). The value of the density iso-surface is 3.0×10^{-3} Å^{-3}.

energy at room temperature (~25 meV).[24] Therefore, if formed, the small polarons would remain highly stable against thermal fluctuations, which precludes a rapid recovery of the photocurrent, contradictory to the experimental observations. (2) The proposal cannot explain the steep temperature dependence (activation law) for the degradation and recovery of the photocurrent, which "needs to be elucidated by future studies" as acknowledged by the authors.

In this paper, we propose an alternative theory that can explain all key experimental observations. Recognizing the importance of light activation and the role of defects in charge transport, we focus on defect-trapped excitons as opposed to small polarons in the pristine material. On the basis of first-principles calculations, our theory can rationalize both the fast and the slow time scales of self-healing, the contrasting dynamics of photocurrent degradation and recovery, and the steep temperature dependence of the competing processes. Some quantitative agreement with the experiments is also reached. We further predict that the same phenomena, i.e., light-activated photocurrent degradation and self-healing, could also be found in other LHPs with even faster time scales of recovery.

In the experiments, the perovskite active layer was solution-processed with large grains.[25,26] As a result, the effect of grain boundaries is not expected to be significant. Thus, in our work, we focus on two representative point defects, lead and iodine vacancies, which are abundant in LHPs under typical synthetic conditions.[27−29] The conclusions drawn from the two vacancies can be generalized to other defects. We are particularly interested in the iodine vacancies because they were shown to be formed under electron beam illumination recently.[30] More importantly, the iodine vacancies are believed to initiate structural decomposition and degradation in $MAPbI_3$ under illumination. Our study could examine whether the same degradation would also occur under photoillumination. Four lead halide perovskites $APbX_3$ [A = methylammonium (MA) or formamidinium (FA), and X = I or Br] in their respective stable phase at room temperature[31−34] are included in the present first-principles calculations. To study defect-trapped excitons, we first perform geometric relaxation in the ground state of the perovskite, after which we further relax the molecular geometry in the excited state of the perovskite by employing a newly developed first-principles approach based on time-dependent density functional theory (TDDFT). The TDDFT approach captures both the electron−hole and electron/hole−nucleus interactions on the same footing.[35] To calculate the density of states (DOS) of the perovskites, we have used both the optimally tuned and range-separated hybrid (OT-RSH) functional[36] and Perdew−Burke−Ernzerhof functional[37] with spin−orbital coupling (SOC). The computational details can be found in the Supporting Information.

In this work, we focus on two point defects, halogen vacancy and lead vacancy, both of which were predicted to have low formation energies.[27,38,39] We first consider the iodine vacancy (V_I) in $MAPbI_3$ by removing an I^- ion from the supercell of 384 atoms, which amounts to an iodine vacancy concentration of 1.2×10^{20} cm^{-3}. Due to the computational costs of the OT-RSH calculations, the vacancy concentration is rather high, although Walsh et al. have shown that the vacancy concentrations in $MAPbI_3$ can actually reach this level.[40] We

DOI: 10.1021/acs.jpclett.9b03413
J. Phys. Chem. Lett. 2019, 10, 7774−7780

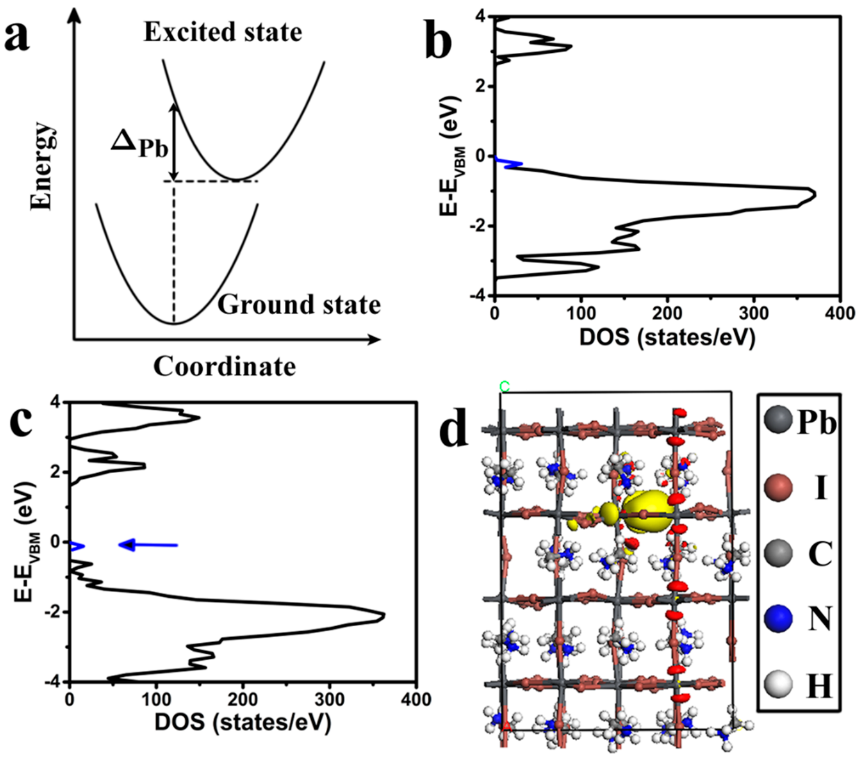

Figure 2. (a) Sketch of the potential energy surfaces in the electronic ground state and the lowest excited state for $MAPbI_3$ in the presence of lead vacancies. Δ_{Pb} is defined in the same way as Δ_1 in Figure 1a. (b) DOS of the system before the forward relaxation with shallow defect levels colored blue. (c) DOS after the forward relaxation with the deep trap states colored blue. The DOS in panels b and c are calculated by the OT-RSH functional. (d) Exciton charge density with the electron (hole) density colored red (yellow). The value of the density iso-surface is 5.0×10^{-3} Å^{-3}.

next calculate the potential energy surfaces (PESs) of the defective $MAPbI_3$ in its electronic ground state and the lowest excited state (shown in Figure 1a), with three energies defined therein. The first is reorganization energy Δ_1 (6 meV), which is defined as the difference in the excitation energies between the equilibrium geometries in the ground state and the excited state. The reorganization energy is analogous to the polaron binding energy and represents self-trapping or stabilization of the exciton. Note that Δ_1 signifies the trapping of a charge-neutral exciton to the defect, whereas the polaron binding energy describes the binding of a charged particle (electron or hole) to lattice deformation in a pristine material. The self-trapping of the exciton is realized via the geometric relaxation in the excited state. In the following, we will term the reorganization energy as the exciton trapping energy. Aside from Δ_1, two energy barriers in the PES of the excited state are of interest to us. Energy Δ_2 (20 meV) represents the energy barrier that the system has to overcome to reach the equilibrium geometry in the excited state from the equilibrium geometry in the ground state. This geometric change will be called "forward relaxation" in the following through which the free exciton becomes trapped by the vacancy. Conversely, the system can also undergo geometric change from the equilibrium geometry in the excited state back to the equilibrium geometry in the ground state, and this process will be termed "backward relaxation", whose energy barrier is Δ_3 (26 meV). The backward relaxation detraps the exciton. Note that a similar energy barrier was also observed in one-dimensional perovskites for self-trapping excitons;[41] thus, this phenomenon, the presence of barriers in excited-state PES, is not unique for V_I in $MAPbI_3$, and our analysis represents a general approach to this type of problem.

The next task is to examine the equilibrium geometry of V_I in its excited state. Interestingly, we find that the Pb^{2+} ion adjacent to V_I is pulled toward the vacancy, weakening and breaking the Pb−I bond on the opposite side of the vacancy (Figure S1). This implies that V_I may initiate structural degradation in $MAPbI_3$ under photoillumination, corroborating the experimental observation that the decomposition of $MAPbI_3$ under electron beam illumination is initiated with the formation of iodine vacancies.[30] We subsequently compare the DOS of the perovskite before and after the forward relaxation, shown in panels b and c of Figure 1. We note that prior to the forward relaxation, shallow defect states are present at the bottom of the conduction band (Figure 1b). However, after the relaxation, deep trap states emerge in the midgap whose energy is >0.8 eV from the conduction band edge (Figure 1c). Therefore, the deep trap states are the result of the forward relaxation upon photoexcitation and are predominantly contributed by lead atoms (Figure S2a). The conclusion remains the same when the SOC correction is included (Figure S3a). In Figure 1d, we display the exciton charge density after the forward relaxation and find it to be highly localized around the vacancy. Therefore, we conclude that photoillumination can indeed lead to structural damage around the vacancy, which in turn generates the localized midgap trap states. Following the relaxation (which is an activated process), the free exciton becomes trapped by the defect. The presence of the light-activated and localized midgap trap states agrees quite well with the experimental observations.[23]

We next turn to the lead vacancy (V_{Pb}) by removing a Pb^{2+} ion from the supercell. In Figure 2a, we present the PESs for the ground state and the lowest excited state, similar to V_I. However, unlike V_I, there is no energy barrier in the excited-

DOI: 10.1021/acs.jpclett.9b03413
J. Phys. Chem. Lett. 2019, 10, 7774−7780

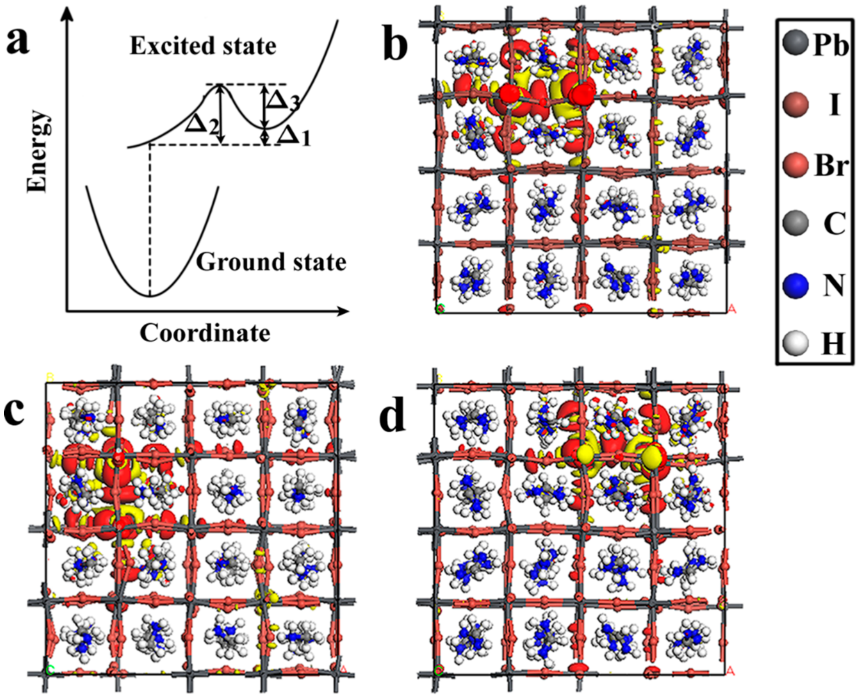

Figure 3. (a) Sketch of the potential energy surfaces in the electronic ground state and the lowest excited state for the three perovskites in the presence of halogen vacancies. Δ_1−Δ_3 are defined in the same way as those in Figure 1a. Exciton charge densities in the presence of halogen vacancies are shown in (b) $FAPbI_3$, (c) $MAPbBr_3$, and (d) $FAPbBr_3$. The electron (hole) density is colored red (yellow). The values of the density iso-surface are (b) 1.5×10^{-3} Å^{-3}, (c) 2.0×10^{-3} Å^{-3}, and (d) 2.0×10^{-3} Å^{-3}.

state PES for V_{Pb}. On the other hand, the exciton trapping energy to V_{Pb} is much higher (Δ_{Pb} = 38 meV), suggesting that the forward relaxation is spontaneous and the exciton is more strongly bound to V_{Pb}. In addition, no light-induced structural damage is observed in the presence of V_{Pb}. Importantly, we find that deep trap states also appear in the DOS after the forward relaxation (Figure 2c), and the trap states contributed predominantly by iodine atoms (Figure S2b) are ∼0.4 eV from the valence band edge. In contrast, no such deep trap states are present before the relaxation (Figure 2b), suggesting that these trap states are induced by the geometric relaxation upon photoexcitation. In Figure 2d, we present the exciton charge density after the geometric relaxation and find it to be localized around V_{Pb}.

With these first-principles results, we can rationalize the key experimental observations. Under photoillumination, free excitons are formed on an ultrafast time scale. Because the exciton binding energy in $MAPbI_3$ is very small (a few millielectronvolts at room temperature),[42] a fraction of the free excitons will dissociate into free carriers on a femtosecond time scale.[43] In fact, the coexistence of excitons and free carriers has been observed experimentally in $MAPbI_3$.[44] The remaining free excitons can then undergo the forward relaxation and become trapped by the defects, forming strongly localized trap states. While the trapping by V_{Pb} is spontaneous, the trapping by V_I is a thermally activated process with an energy barrier (Δ_2 = 20 meV). At the same time, the trapped excitons can also escape from the defects and become detrapped. This reversal (or recovery) process is realized by the backward relaxation with the activation energy of Δ_3 (26 meV) for V_I and Δ_{Pb} (38 meV) for V_{Pb}. Therefore, the photocurrent degradation and recovery are determined by the competition between the forward and backward relaxations, i.e., trapping and detrapping.

Let us consider V_I first. Because of a constant supply of newly formed free excitons under the solar illumination, the excitons going forward (trapped) outnumber those going backward (detrapped); thus, the forward process outcompetes the backward process despite their similar energy barriers ($\Delta_2 \approx \Delta_3$). Therefore, more and more excitons become trapped and space charges accumulate in the material, degrading the photocurrent. The competition between the trapping and detrapping and the loss of excitons into free carriers underlie the slow dynamics of photocurrent degradation. When the system is in the dark, the situation is reversed. The backward process now dominates the forward process because the detrapped excitons could dissociate into free carriers. Without the supply of free excitons, the excitons going backward (detrapped) outnumber those going forward (trapped), leading to the gradual disappearance of space charges and recovery of the photocurrent. Because the detrapping energy barrier Δ_3 (26 meV) is comparable to the room-temperature barrier, the backward process can proceed quickly and is assisted by the thermal fluctuations. Every time when excitons become detrapped, a fraction of them disappears into free carriers; thus, the number of excitons going forward (trapped) decays exponentially. In other words, detrapping would dominate trapping, which explains the much faster recovery dynamics of the photocurrent.

A similar but simpler process is at work for V_{Pb}. Under the constant illumination, more and more excitons are trapped by V_{Pb}, following the spontaneous forward relaxation. Thus, the degradation due to V_{Pb} is expected to be faster than that due to V_I. On the other hand, the trapped excitons can also escape from the V_{Pb}, albeit at a slower rate owing to the higher trapping energy Δ_{Pb} (38 meV). Therefore, we can expect two time scales for self-healing of the photocurrent: a faster one

DOI: 10.1021/acs.jpclett.9b03413
J. Phys. Chem. Lett. 2019, 10, 7774−7780

associated with excitons detrapped from V_I and a slower one from V_{Pb}.

Although we have tried to correlate the dynamics of exciton trapping/detrapping to the dynamics of photocurrent degradation/recovery in the preceding analysis, they are conceptionally different and should be distinguished. The microscopic dynamics of exciton trapping/detrapping is very fast and concerns a single defect (or exciton). In contrast, the dynamics of the photocurrent degradation/recovery is determined by the macroscopic process of space charge accumulation/disappearance and, hence, is much slower and involves all defects (or excitons) in the material. Unfortunately, we do not have a means to estimating the dynamics of space charge accumulation/disappearance from first principles, which likely depends on the configurations of the defects, space charges, and their long-range interactions.

One important experimental observation is that both the degradation and the recovery processes depend sensitively on temperature, particularly for photodegradation. This suggests that the underlying processes are thermally activated whose energy barriers must be comparable to the temperature. Finally, we note that the drop in V_{oc} (40 mV) coincides with the highest value of the relevant energy barriers (Δ_{Pb} = 38 meV). The coincidence calls for future studies to elucidate the roles of V_{Pb} in affecting the V_{oc} of the devices. Although we do not examine all defects in $MAPbI_3$, our conclusions are expected to be valid for other defects, as well. This is because while characteristic energies could be different for different defects, the general phenomenon is the same. The excited-state PESs can have barriers (like V_I) or no barriers (like V_{Pb}), but both are included in our theory.

Having explained all key experimental observations in $MAPbI_3$, we next ask whether the same phenomena can also be realized in other LHPs. To this end, we consider $FAPbI_3$, $MAPbBr_3$, and $FAPbBr_3$, which are related to $MAPbI_3$ via the replacement of MA cation with FA cation and iodine ion with bromine ion, respectively. Both halogen vacancies (V_I and V_{Br}) and lead vacancies are examined. When the halogen vacancies are introduced, we find that the PES of the excited state exhibits the similar behavior as in $MAPbI_3$ with activated processes, but with a reversed asymmetry of the energy barriers (Figure 3a). More specifically, the forward barrier (Δ_2) is greater than the backward barrier (Δ_3) with a negative exciton trapping energy (Δ_1). The values of these energies are listed in Table 1.

Similar to $MAPbI_3$, the free excitons in the three LHPs can be trapped by the halogen vacancies following forward relaxation. The emergence of localized midgap trap states is apparent from the exciton charge density in Figure 3 and DOS in Figures S3 and S4. The similar bond weakening/breaking in the vicinity of halogen vacancies is also observed in these perovskites with the halogen vacancies (Figure S5). However, unlike $MAPbI_3$, the trapped excitons are energetically less stable than the free excitons with negative Δ_1 values. Importantly, the detrapping energy barrier (Δ_3) is between 12 and 15 meV, smaller than the corresponding value in $MAPbI_3$. Thus, if the localized trap states are formed in these LHPs, their recovery dynamics is predicted to be faster than that in $MAPbI_3$.

The same conclusion holds when we consider V_{Pb} in the three perovskites. Similar to $MAPbI_3$, no energy barrier is present in the excited-state PES for these perovskites with V_{Pb}, and the formation of trapped excitons is spontaneous. However, the trapping energy (Δ_{Pb}) is 1.6, 6.1, and 1.2 meV in $FAPbI_3$, $MAPbBr_3$, and $FAPbBr_3$, respectively (Table 1), which is much smaller than the trapping energy (38 meV) in $MAPbI_3$. In fact, no deep trap states are observed in these perovskites owing to their vanishingly small trapping energies. Therefore, the excitons are essentially free in the presence of V_{Pb} and can dissociate into free charge carriers. In other words, no photocurrent degradation is expected in these perovskites due to the presence of V_{Pb}. Overall, we predict the higher photostability in $FAPbI_3$, $MAPbBr_3$, and $FAPbBr_3$, which is manifested by the absence of photocurrent degradation due to V_{Pb} and faster self-healing dynamics due to the halogen vacancies. This trend is in line with the experimental finding that perovskites with FA cations generally exhibit markedly longer carrier diffusion lengths than the MA counterparts.[45] Finally, we also note an interesting correlation between the lattice stiffness (e.g., Young's modulus) and photostability (Table 1). The more stable $FAPbI_3$, $MAPbBr_3$, and $FAPbBr_3$ have Young's moduli that are higher than that of $MAPbI_3$, suggesting that one may be able to enhance the photostability of the perovskites by tuning their chemical compositions.

To summarize, we provide a first-principles theory that can elucidate the key experimental observations on light-activated photocurrent degradation and self-healing in $MAPbI_3$. It is revealed that upon photoexcitation, structural changes take place, which leads to the formation of localized excitons trapped at the defects. Under constant illumination, the deep trap states accumulate to yield space charge distribution and result in photocurrent degradation. In the presence of V_I, both photoinduced structural relaxation and its reversal are activated processes with energy barriers (20 and 26 meV, respectively) comparable to the room-temperature value. In the presence of V_{Pb}, on the other hand, the photoinduced structural relaxation is spontaneous and the exciton trapping energy (38 meV) is higher than the room-temperature value. By considering that the detrapped excitons can dissociate into free carriers, the theory can also explain the contrasting dynamics between the photodegradation and the recovery. Finally, we predict that $FAPbI_3$, $MAPbBr_3$, and $FAPbBr_3$ can exhibit behavior similar to that of $MAPbI_3$, but with faster recovery dynamics.

Table 1. Summary of the Energies (millielectronvolts) Defined in Figures 1a−3a[a]

	$MAPbI_3$	$FAPbI_3$	$MAPbBr_3$	$FAPbBr_3$
Δ_1	6	−10	−6	−13
Δ_2	20	22	21	28
Δ_3	26	12	15	15
Δ_{Pb}	38	1.6	6.1	1.2
E	34.8	41.8	49.9	45.7

[a]The last row shows the effective Young's modulus (E) in GPa defined as $E = (c_{11} + c_{22} + c_{33})/3$, where c_{11}, c_{22}, and c_{33} are elastic constants.

■ ASSOCIATED CONTENT

Supporting Information

The Supporting Information is available free of charge at https://pubs.acs.org/doi/10.1021/acs.jpclett.9b03413.

Computational details and method, experimental cell parameters and band structures of the studied perovskites, atomic structures of the perovskites in the

DOI: 10.1021/acs.jpclett.9b03413
J. Phys. Chem. Lett. 2019, 10, 7774−7780

presence of halogen vacancies, and DOS and partial DOS calculated at different levels (PDF)

AUTHOR INFORMATION

Corresponding Author

*E-mail: ganglu@csun.edu.

ORCID

Guangjun Nan: 0000-0002-5185-8336

Xu Zhang: 0000-0002-6491-3234

Gang Lu: 0000-0002-9168-8968

Notes

The authors declare no competing financial interest.

ACKNOWLEDGMENTS

G.N. acknowledges the support by the Natural Science Foundation of Zhejiang Province in China (LY20A040003). The work at California State University, Northridge, was supported by the U.S. National Science Foundation (DMR1828019) and the U.S. Army Research Office (W911NF1810473).

REFERENCES

(1) Grätzel, M. The Rise of Highly Efficient and Stable Perovskite Solar Cells. *Acc. Chem. Res.* **2017**, *50*, 487−491.

(2) Manser, J. S.; Christians, J. A.; Kamat, P. V. Intriguing Optoelectronic Properties of Metal Halide Perovskites. *Chem. Rev.* **2016**, *116*, 12956−13008.

(3) Li, J.; Xu, L.; Wang, T.; Song, J.; Chen, J.; Xue, J.; Dong, Y.; Cai, B.; Shan, Q.; Han, B.; Zeng, H. 50-Fold EQE Improvement up to 6.27% of Solution-Processed All-Inorganic Perovskite $CsPbBr_3$ QLED via Surface Ligand Density Control. *Adv. Mater.* **2017**, *29*, 1603885.

(4) Lin, K.; Xing, J.; Quan, L. N.; García de Arquer, F. P.; Gong, X.; Lu, J.; Xie, L.; Zhao, W.; Zhang, D.; Yan, C.; Li, W.; Liu, X.; Lu, Y.; Kirman, J.; Sargent, E. H.; Xiong, Q.; Wei, Z. Perovskite Light-Emitting Diodes with External Quantum Efficiency Exceeding 20 Percent. *Nature* **2018**, *562*, 245−248.

(5) Zhu, H.; Fu, Y.; Meng, F.; Wu, X.; Gong, Z.; Ding, Q.; Gustafsson, M. V.; Tuan Trinh, M.; Jin, S.; Zhu, X.-Y. Lead Halide Perovskite Nanowire Lasers with Low Lasing Thresholds and High Quality Factors. *Nat. Mater.* **2015**, *14*, 636−642.

(6) Bisquert, J. The Swift Surge of Perovskite Photovoltaics. *J. Phys. Chem. Lett.* **2013**, *4*, 2597−2598.

(7) Best Research-Cell Efficient Chart by NREL. https://www.nrel.gov/pv/assets/pdfs/best-research-cell-efficiencies.20191106.pdf.

(8) Christians, J. A.; Miranda Herrera, P. A.; Kamat, P. V. Transformation of the Excited State and Photovoltaic Efficiency of $CH_3NH_3PbI_3$ Perovskite upon Controlled Exposure to Humidified Air. *J. Am. Chem. Soc.* **2015**, *137*, 1530−1538.

(9) Mosconi, E.; Azpiroz, J. M.; De Angelis, F. Ab Initio Molecular Dynamics Simulations of Methylammonium Lead Iodide Perovskite Degradation by Water. *Chem. Mater.* **2015**, *27*, 4885−4892.

(10) Leijtens, T.; Eperon, G. E.; Pathak, S.; Abate, A.; Lee, M. M.; Snaith, H. J. Overcoming Ultraviolet Light Instability of Sensitized TiO_2 with Meso-Superstructured Organometal Tri-halide Perovskite Solar Cells. *Nat. Commun.* **2013**, *4*, 2885.

(11) Qin, C.; Matsushima, T.; Fujihara, T.; Potscavage, W. J., Jr.; Adachi, C. Degradation Mechanisms of Solution-Processed Planar Perovskite Solar Cells: Thermally Stimulated Current Measurement for Analysis of Carrier Traps. *Adv. Mater.* **2016**, *28*, 466−471.

(12) Reyes-Martinez, M. A.; Abdelhady, A. L.; Saidaminov, M. I.; Chung, D. Y.; Bakr, O. M.; Kanatzidis, M. G.; Soboyejo, W. O.; Loo, Y.-L. Time-Dependent Mechanical Response of $APbX_3$ (A = Cs, CH_3NH_3; X = I, Br) Single Crystals. *Adv. Mater.* **2017**, *29*, 1606556.

(13) Noel, N. K.; Abate, A.; Stranks, S. D.; Parrott, E. S.; Burlakov, V. M.; Goriely, A.; Snaith, H. J. Enhanced Photoluminescence and Solar Cell Performance via Lewis Base Passivation of Organic-Inorganic Lead Halide Perovskites. *ACS Nano* **2014**, *8*, 9815−9821.

(14) Abdi-Jalebi, M.; Andaji-Garmaroudi, Z.; Cacovich, S.; Stavrakas, C.; Philippe, B.; Richter, J. M.; Alsari, M.; Booker, E. P.; Hutter, E. M.; Pearson, A. J.; Lilliu, S.; Savenije, T. J.; Rensmo, H.; Divitini, G.; Ducati, C.; Friend, R. H.; Stranks, S. D. Maximizing and Stabilizing Luminescence from Halide Perovskites with Potassium Passivation. *Nature* **2018**, *555*, 497−501.

(15) Snaith, H. J. Present Status and Future Prospects of Perovskite Photovoltaics. *Nat. Mater.* **2018**, *17*, 372−376.

(16) Leijtens, T.; Bush, K. A.; Prasanna, R.; McGehee, M. D. Opportunities and Challenges for Tandem Solar Cells Using Metal Halide Perovskite Semiconductors. *Nat. Energy* **2018**, *3*, 828−838.

(17) Zhou, Y.; You, L.; Wang, S.; Ku, Z.; Fan, H.; Schmidt, D.; Rusydi, A.; Chang, L.; Wang, L.; Ren, P.; Chen, L.; Yuan, G.; Chen, L.; Wang, J. Giant Photostriction in Organic-Inorganic Lead Halide Perovskites. *Nat. Commun.* **2016**, *7*, 11193.

(18) Berhe, T. A.; Su, W.-N.; Chen, C.-H.; Pan, C.-J.; Cheng, J.-H.; Chen, H.-M.; Tsai, M.-C.; Chen, L.-Y.; Dubale, A. A.; Hwang, B.-J. Organometal Halide Perovskite Solar Cells: Degradation and Stability. *Energy Environ. Sci.* **2016**, *9*, 323−356.

(19) Li, B.; Li, Y.; Zheng, C.; Gao, D.; Huang, W. Advancements in the Stability of Perovskite Solar Cells: Degradation Mechanisms and Improvement Approaches. *RSC Adv.* **2016**, *6*, 38079−38091.

(20) Galisteo-López, J. F.; Li, Y.; Míguez, H. Three-Dimensional Optical Tomography and Correlated Elemental Analysis of Hybrid Perovskite Microstructures: An Insight into Defect-Related Lattice Distortion and Photoinduced Ion Migration. *J. Phys. Chem. Lett.* **2016**, *7*, 5227−5234.

(21) deQuilettes, D. W.; Zhang, W.; Burlakov, V. M.; Graham, D. J.; Leijtens, T.; Osherov, A.; Bulović, V.; Snaith, H. J.; Ginger, D. S.; Stranks, S. D. Photo-Induced Halide Redistribution in Organic-Inorganic Perovskite Films. *Nat. Commun.* **2016**, *7*, 11683.

(22) Mosconi, E.; Meggiolaro, D.; Snaith, H. J.; Stranks, S. D.; De Angelis, F. Light-Induced Annihilation of Frenkel Defects in Organo-Lead Halide Perovskites. *Energy Environ. Sci.* **2016**, *9*, 3180−3187.

(23) Nie, W.; Blancon, J.-C.; Neukirch, A. J.; Appavoo, K.; Tsai, H.; Chhowalla, M.; Alam, M. A.; Sfeir, M. Y.; Katan, C.; Even, J.; Tretiak, S.; Crochet, J.; Gupta, G.; Mohite, A. D. Light-Activated Photocurrent Degradation and Self-Healing in Perovskite Solar Cells. *Nat. Commun.* **2016**, *7*, 11574.

(24) Neukirch, A. J.; Nie, W.; Blancon, J.-C.; Appavoo, K.; Tsai, H.; Sfeir, M. Y.; Katan, C.; Pedesseau, L.; Even, J.; Crochet, J. J.; Gupta, G.; Mohite, A. D.; Tretiak, S. Polaron Stabilization by Cooperative Lattice Distortion and Cation Rotations in Hybrid Perovskite Materials. *Nano Lett.* **2016**, *16*, 3809−3816.

(25) Nie, W.; Tsai, H.; Asadpour, R.; Blancon, J.-C.; Neukirch, A. J.; Gupta, G.; Crochet, J. J.; Chhowalla, M.; Tretiak, S.; Alam, M. A.; Wang, H.-L.; Mohite, A. D. High-Efficiency Solution-Processed Perovskite Solar Cells with Millimeter-Scale Grains. *Science* **2015**, *347*, 522−525.

(26) Dong, Q.; Fang, Y.; Shao, Y.; Mulligan, P.; Qiu, J.; Cao, L.; Huang, J. Electron-Hole Diffusion Lengths > 175 μm in Solution-Grown $CH_3NH_3PbI_3$ Single Crystals. *Science* **2015**, *347*, 967−970.

(27) Buin, A.; Comin, R.; Xu, J.; Ip, A. H.; Sargent, E. H. Halide-Dependent Electronic Structure of Organolead Perovskite Materials. *Chem. Mater.* **2015**, *27*, 4405−4412.

(28) Yin, W.-J.; Shi, T.; Yan, Y. Superior Photovoltaic Properties of Lead Halide Perovskites: Insights from First-Principles Theory. *J. Phys. Chem. C* **2015**, *119*, 5253−5264.

(29) Meggiolaro, D.; Motti, S. G.; Mosconi, E.; Barker, A. J.; Ball, J.; Andrea Riccardo Perini, C.; Deschler, F.; Petrozza, A.; De Angelis, F. Iodine Chemistry Determines the Defect Tolerance of Lead-Halide Perovskites. *Energy Environ. Sci.* **2018**, *11*, 702−713.

(30) Chen, S.; Zhang, X.; Zhao, J.; Zhang, Y.; Kong, G.; Li, Q.; Li, N.; Yu, Y.; Xu, N.; Zhang, J.; Liu, K.; Zhao, Q.; Cao, J.; Feng, J.; Li, X.; Qi, J.; Yu, D.; Li, J.; Gao, P. Atomic Scale Insights into Structure Instability and Decomposition Pathway of Methylammonium Lead Iodide Perovskite. *Nat. Commun.* **2018**, *9*, 4807.

DOI: 10.1021/acs.jpclett.9b03413
J. Phys. Chem. Lett. 2019, 10, 7774−7780

(31) Poglitsch, A.; Weber, D. Dynamic Disorder in Methylammoniumtrihalogenoplumbates (II) Observed by Millimeter-Wave Spectroscopy. *J. Chem. Phys.* **1987**, *87*, 6373−6378.

(32) Weller, M. T.; Weber, O. J.; Frost, J. M.; Walsh, A. Cubic Perovskite Structure of Black Formamidinium Lead Iodide, α-$[HC(NH_2)_2]PbI_3$, at 298 K. *J. Phys. Chem. Lett.* **2015**, *6*, 3209−3212.

(33) Page, K.; Siewenie, J. E.; Quadrelli, P.; Malavasi, L. Short-Range Order of Methylammonium and Persistence of Distortion at the Local Scale in $MAPbBr_3$ Hybrid Perovskite. *Angew. Chem., Int. Ed.* **2016**, *55*, 14320−14324.

(34) Zhumekenov, A. A.; Saidaminov, M. I.; Haque, M. A.; Alarousu, E.; Sarmah, S. P.; Murali, B.; Dursun, I.; Miao, X.-H.; Abdelhady, A. L.; Wu, T.; Mohammed, O. F.; Bakr, O. M. Formamidinium Lead Halide Perovskite Crystals with Unprecedented Long Carrier Dynamics and Diffusion Length. *ACS Energy Lett.* **2016**, *1*, 32−37.

(35) Zhang, X.; Lu, G. Subspace Formulation of Time-Dependent Density Functional Theory for Large-Scale Calculations. *J. Chem. Phys.* **2015**, *143*, 064110.

(36) Refaely-Abramson, S.; Jain, M.; Sharifzadeh, S.; Neaton, J. B.; Kronik, L. Solid-State Optical Absorption from Optimally Tuned Time-Dependent Range-Separated Hybrid Density Functional Theory. *Phys. Rev. B: Condens. Matter Mater. Phys.* **2015**, *92*, No. 081204(R).

(37) Perdew, J. P.; Burke, K.; Ernzerhof, M. Generalized Gradient Approximation Made Simple. *Phys. Rev. Lett.* **1996**, *77*, 3865−3868.

(38) Meggiolaro, D.; De Angelis, F. First-Principles Modeling of Defects in Lead Halide Perovskites: Best Practices and Open Issues. *ACS Energy Lett.* **2018**, *3*, 2206−2222.

(39) Yin, W.-J.; Shi, T.; Yan, Y. Unusual Defect Physics in $CH_3NH_3PbI_3$ Perovskite Solar Cell Absorber. *Appl. Phys. Lett.* **2014**, *104*, 063903.

(40) Walsh, A.; Scanlon, D. O.; Chen, S.; Gong, X. G.; Wei, S.-H. Self-Regulation Mechanism for Charged Point Defects in Hybrid Halide Perovskites. *Angew. Chem., Int. Ed.* **2015**, *54*, 1791−1794.

(41) Wang, X.; Meng, W.; Liao, W.; Wang, J.; Xiong, R.-G.; Yan, Y. Atomistic Mechanism of Broadband Emission in Metal Halide Perovskites. *J. Phys. Chem. Lett.* **2019**, *10*, 501−506.

(42) Miyata, A.; Mitioglu, A.; Plochocka, P.; Portugall, O.; Wang, J. T.-W.; Stranks, S. D.; Snaith, H. J.; Nicholas, R. J. Direct Measurement of the Exciton Binding Energy and Effective Masses for Charge Carriers in Organic-Inorganic Tri-halide Perovskites. *Nat. Phys.* **2015**, *11*, 582−587.

(43) Jha, A.; Duan, H.-G.; Tiwari, V.; Nayak, P. K.; Snaith, H. J.; Thorwart, M.; Miller, R. J. D. Direct Observation of Ultrafast Exciton Dissociation in Lead Iodide Perovskite by 2D Electronic Spectroscopy. *ACS Photonics* **2018**, *5*, 852−860.

(44) D'Innocenzo, V.; Grancini, G.; Alcocer, M. J. P.; Kandada, A. R. S.; Stranks, S. D.; Lee, M. M.; Lanzani, G.; Snaith, H. J.; Petrozza, A. Excitons versus Free Charges in Organo-Lead Tri-halide Perovskites. *Nat. Commun.* **2014**, *5*, 3586.

(45) Zhumekenov, A. A.; Saidaminov, M. I.; Haque, M. A.; Alarousu, E.; Sarmah, S. P.; Murali, B.; Dursun, I.; Miao, X.-H.; Abdelhady, A. L.; Wu, T.; Mohammed, O. F.; Bakr, O. M. Formamidinium Lead Halide Perovskite Crystals with Unprecedented Long Carrier Dynamics and Diffusion Length. *ACS Enegy Lett.* **2016**, *1*, 32−37.

DOI: 10.1021/acs.jpclett.9b03413
J. Phys. Chem. Lett. 2019, 10, 7774−7780